Supporting Information

Sharp et al. 10.1073/pnas.1118622109

SI Text

SI Materials and Methods. ***Peptide synthesis.*** Peptides were synthesised on a 0.1 mmol scale using $O-(\text{Benzotriazol}-1-\text{y1})-N,N,N',N'$–tetramethyluronium hexafluorophosphate (HBTU) activation on a CEM Liberty synthesizer (CEM Corp.). All standard Fmoc amino acids and reagents were purchased from AGTC Bioproducts. Fmoc 4-iodophenylalanine was purchased from GL Biochem. Peptide synthesis grade DMF was purchased from Fisher Scientific. Peptides were prepared using a Wang-Chemmatrix solid support (PCAS Biomatrix), which was either bought preloaded or was loaded using a DIC/HOBt/DMAP method recommended by the manufacturer. Crude peptides were cleaved from the solid support by treatment with a 95:2.5:2.5 mix of TFA:water:triispropylsilane (10 mL) for 2 h at room temperature, followed by an additional wash of the resin with neat TFA (10 mL). The combined TFA extracts were reduced in volume to *ca*. 5 mL under a gentle flow of nitrogen prior to the addition of cold diethyl ether (*ca*. 45 mL). The resultant precipitate was isolated by centrifugation and then dissolved in 1:1 water:acetonitrile and freeze-dried to give the crude peptide as a fluffy white solid. Crude peptides were purified by reverse-phase HPLC using a Kromatek Hi-Q Sil semipreparative C18 column running a linear gradient of water and acetonitrile buffers, each containing 0.1% TFA. Gradients were typically runs from 20% to 60% acetonitrile over 30 min. Pure column fractions were identified by MALDI-TOF mass spectrometry, using an Applied Biosystems 4700 Series Proteomics Analyzer instrument. Pure fractions were combined and freeze-dried, with the purity of the resultant material being checked by analytical HPLC. Concentration of peptides were determined by UV-visible spectroscopy, with molar extinction coefficients of $\varepsilon_{274}(\text{Tyr}) = 1420\ \text{M}^{-1}\,\text{cm}^{-1}$ and $\varepsilon_{280}(p\text{-iodo-phenylalanine}) = 260\ \text{M}^{-1}\,\text{cm}^{-1}$. The sequences of the peptides can be found in Table S2.

X-ray crystal structure determination. Freeze-dried peptides were resuspended directly into deionized water and concentrated to 10 mg/mL for vapor-diffusion crystallization trials using standard commercial screens at 18 °C with 0.2 μL peptide equilibrated with 0.2 μL of reservoir solution. The crystallization conditions were 0.2 M zinc acetate, 0.1 M sodium acetate, and 10% (wt/vol) PEG 3 K, at pH 4.5. X-ray diffraction data were collected at the Diamond Light Source on station IO4 using radiation of 1.7 Å wavelength. The data were processed with HKL2000 (1). The structure was solved with SHELX (2) by experimental phasing using single anomalous diffraction (SAD) from the iodine atoms. Four clear α-helixes could be identified in the resultant electron density map. The model was automatically built using ARP/wARP (3) and Phenix Autobuild software (4). The final refined structure was obtained by subsequent iterative model building with the program COOT (5), and refinement with REFMAC (6) and PHENIX (7). Translation Libration Screw-motion (TLS) parameters were used in the final rounds of refinement, with one TLS group assigned to each protein chain. The final model includes one ion, identified from the density and coordination as a zinc, and a glycerol molecule, both prevalent components of the crystallization buffer. A summary of the refinement and model-building statistics can be found together with Protein Data Bank (PDB) accession codes in Table S3.

Model building and fitting. Coiled coils were modeled using MAKECCSC with a radius of 4.4 Å, a rise per residue (t_{res}) of 1.529 Å, and a $\varphi_{C\beta}$ of 210°, as defined by Offer and Sessions (7). The value for t_{res} was chosen so that equivalent residues had the same x, y coordinates after each pitch.

The EM density map produced from helical reconstruction was thresholded to enclose the volume of either 100% or 60% of the mass of the protein model. The values were calculated based on the weight of three heterodimers (19,496 Da, corresponding to a single pitch of the coiled coil) multiplied by 1.21 $\text{Å}^3\,\text{Da}^{-1}$ (8). Atomic models were fitted into the EM density map as rigid structures. Chimera (University of California, San Francisco) (9) was used first to place manually the model within the EM density map before simulating the PDB model density to 8 Å and optimizing the correlation between the two maps. The fitting routine was repeated until convergence. Different starting orientations were also tried.

Molecular-dynamics simulation. One pitch of coiled coil was modeled as a sticky-ended repeat unit, derived from the 3_1 helix above, containing three copies of each peptide. Intracoiled-coil side-chain conformations were set to those of the blunt-ended crystal structure. Intercoiled-coil side chains were left in an extended conformation at this stage. A hexagonal 1 by 3 by 3 repeating cell of these repeat units was generated. Minimal alterations to the intercoiled-coil side-chain torsions were made, by inspection, to remove clashes and maximize Arg:Asp salt bridges. All structural manipulations were performed using InsightII (2005; Accelrys Inc.) and PyMol (available at www.pymol.org). This unit cell was used as the box for an all-atom molecular-dynamics simulation under the AMBER03 force field. The simulation was set up using the GROMACS 4.5.4 suite of tools (available at www.gromacs.org) with side chains charged consistent with pH 7.4, solvated with 6,170 TIP4P waters and neutralized with chloride ions. The system was subjected to 5,000 steps of steepest descent minimization, followed by 5 ns of position-restrained molecular dynamics as an initial equilibration. Unrestrained molecular dynamics was performed for 120 ns at 278 K under periodic boundary conditions (particle mesh Ewald treatment of long range electrostatics) as an NPT ensemble.

Cryotransmission electron microscopy (cryo-TEM) and tomography. Samples were spread on freshly glow-discharged lacey-carbon grids and plunge-frozen in liquid ethane using the Vitrobot (FEI Company). Grids were transferred to a cryoholder (Gatan Inc.) and visualized in a Tecnai T20 electron microscope (FEI Company) at 200 kV accelerating voltage at a nominal magnification of × 50 k. Low-dose software (FEI Company) was used with an underfocus of 1.5 μm and an electron dose of 10 $\text{e}/\text{Å}^2$. Images were captured on an Eagle 4 k by 4 k CCD camera (FEI Company) unbinned with a final pixel size of 2.21 Å. The EM was calibrated with a negatively stained catalase crystal and a sample of graphitized carbon. A sample of T4 bacteriophage, with a tail striation of 40.6 Å (10), was incubated with fully formed SAFs for 30 s prior to addition to grids and freezing. For tomography, lacey-carbon grids were incubated with 15 nm colloidal gold (Aurion) on both sides to act as fiducial markers. Samples were plunge-frozen as described above.

1. Otwinowski Z, Minor W (1997) Processing of X-ray diffraction data collected in oscillation mode. *Methods Enzymol* 276:307–326.
2. Sheldrick GM (2008) A short history of SHELX. *Acta Crystallogr Sect A* 64:112–122.
3. Perrakis A, Harkiolaki M, Wilson KS, Lamzin VS (2001) ARP/wARP and molecular replacement. *Acta Crystallogr Sect D-Biol Crystallogr* 57:1445–1450.

4. Adams PD, et al. (2010) PHENIX: A comprehensive Python-based system for macromolecular structure solution. *Acta Crystallogr Sect D-Biol Crystallogr* 66:213–221.
5. Emsley P, Cowtan K (2004) Coot: Model-building tools for molecular graphics. *Acta Crystallogr Sect D-Biol Crystallogr* 60:2126–2132.
6. Murshudov GN, Vagin AA, Dodson EJ (1997) Refinement of macromolecular structures by the maximum-likelihood method. *Acta Crystallogr Sect D-Biol Crystallogr* 53:240–255.
7. Offer G, Sessions R (1995) Computer modeling of the alpha-helical coiled-coil—packing of side-chains in the inner-core. *J Mol Biol* 249:967–987.
8. Harpaz Y, Gerstein M, Chothia C (1994) Volume changes on protein-folding. *Structure* 2:641–649.
9. Goddard TD, Huang CC, Ferrin TE (2007) Visualizing density maps with UCSF Chimera. *J Struct Biol* 157:281–287.
10. Moody MF, Makowski L (1981) X-ray diffraction study of tail-tubes from bacteriophage-T2l. *J Mol Biol* 150:217–244.

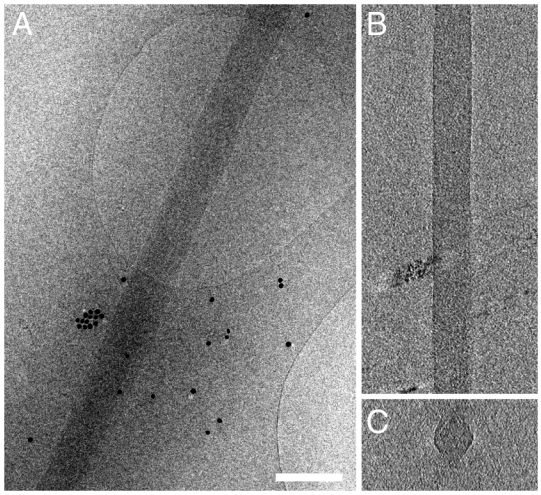

Fig. S1. A tomogram of frozen-hydrated self-assembling peptide fibers (SAFs). (*A*) Image of a SAF used to collect a tomogram from ±45°. The lacey-carbon and gold fiducial markers used to aid reconstruction are clearly visible. (*B*) Orthogonal slice through the fiber in *A*, showing the uniform density present in the interior of the fiber. The image is an average of 30 tomographic slices to aid contrast. (*C*) View along the fiber long-axis showing the approximately circular cross-section of the fiber. Scale bar, 200 nm for all images.

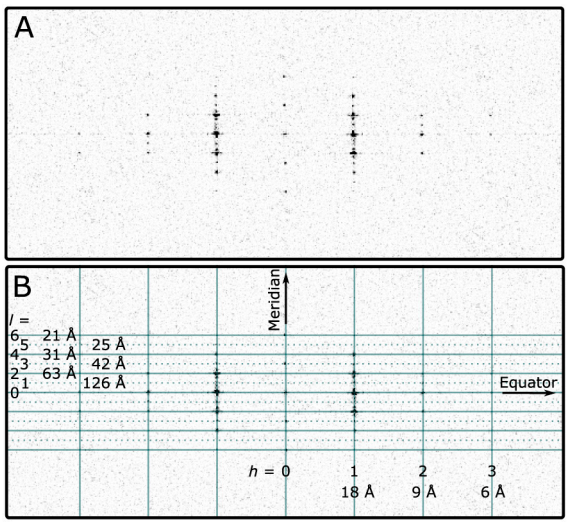

Fig. S2. Fourier transform of the [100] longitudinal striations. (*A*) Background-subtracted Fourier transform of the SAF in Fig. 3 (annotated *B*) with layer and row lines. The first meridional reflection is the third at 41.8 Å. The layer lines (*l*) extend past the sixth at 20.9 Å, whereas row lines (*h*) extend out to the third at 6 Å.

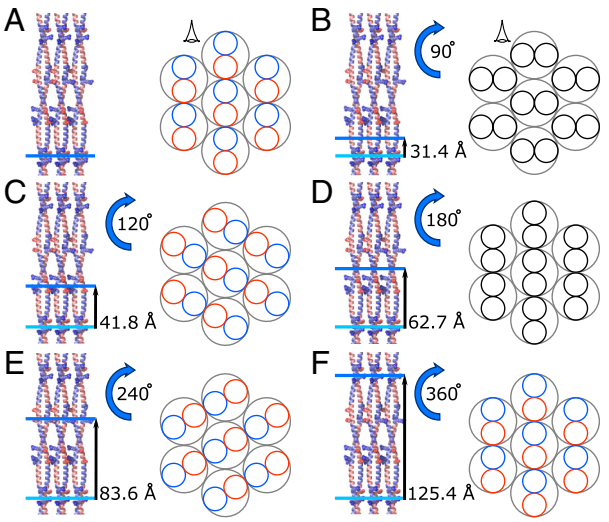

Fig. S3. Cartoon representation of charge-mediated hexagonal packing. Small circles represent α-helices within the coiled coil (large grey circles) and are colored by charge where Arg or Asp residues occur (blue and red circles, respectively). (*A*) Looking through the SAFs (eye symbol) along the [100] axis at the level of the horizontal bar shows basic and acidic residues forming intercoiled-coil interactions. (*B*) After translating 31.35 Å along the SAF, the α-helices have rotated 90° within the coiled coil. (*C*) The α-helices have rotated 120° after 41.8 Å from *A*, where there is another set of intercoiled-coil interactions. (*D*) After half a pitch (63 Å) the α-helices are again aligned with the imaging axis, and longitudinal striations result. (*E*) Intercoiled-coil interactions occur once more in the pitch before the coiled coil has completed a full rotation (*F*).

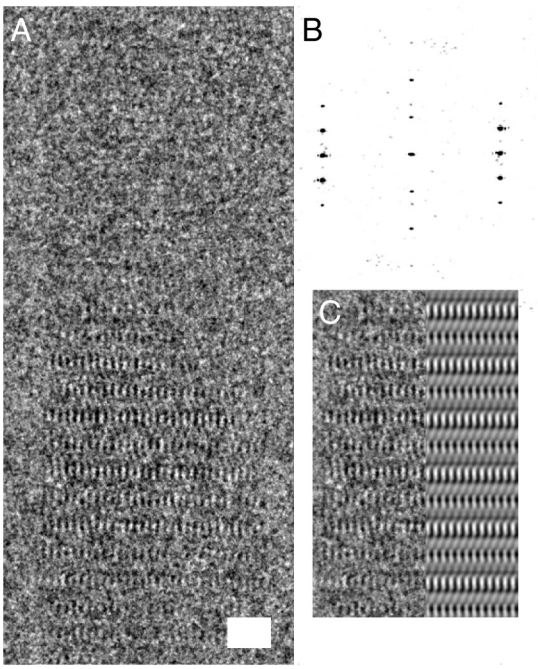

Fig. S4. Iodonated peptides are fiber-competent. (*A*) Cryo-TEM image of a fiber formed from SAF-p1-I and SAF-p2a. SAF-p1-I is the fiber-competent iodinated SAF peptide (Table S2). (*B*) Fourier transform showing equatorial and meridional reflections identical to the fiber formed from non-iodonated peptides, confirming identical hexagonal packing. (*C*) 2dx-processed image of area of fiber in (*A*), showing the lateral striations every 41.8 Å. Scale bar is 10 nm for both (*A*) and (*C*).

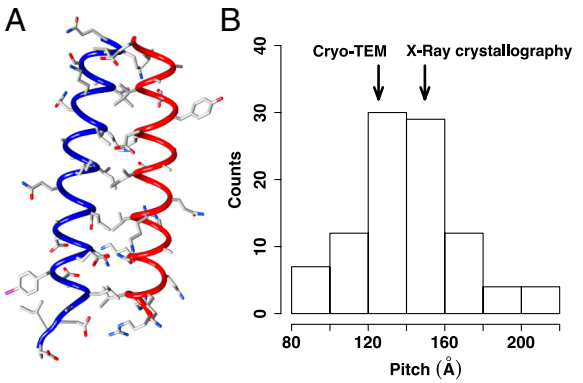

Fig. S5. Structural analysis of the standard and permuted SAF peptides. (*A*) X-ray crystal structure (PDB code 3RA3) of the complex between Blunt-p1-I (blue) and SAF-p2a (red). The structure shows canonical coiled-coil interactions, including salt bridges and the hydrophobic core. (*B*) Histogram showing the pitch variation for manually validated parallel dimeric coiled-coil structures deposited in the PDB ($n = 98$) (1, 2). The pitches of the models derived from cryo-TEM of the SAFs and from X-ray crystallography of the Blunt-p1-I:SAF-p2a complex are also shown at 125.4 Å and 143 Å, respectively.

1 Armstrong CT, Vincent TL, Green PJ, Woolfson DN (2011) SCORER 2.0: An algorithm for distinguishing parallel dimeric and trimeric coiled-coil sequences. *Bioinformatics* 27:1908–1914.
2 Testa OD, Moutevelis E, Woolfson DN (2009) CC plus: A relational database of coiled-coil structures. *Nucleic Acids Res* 37:D315–D322.

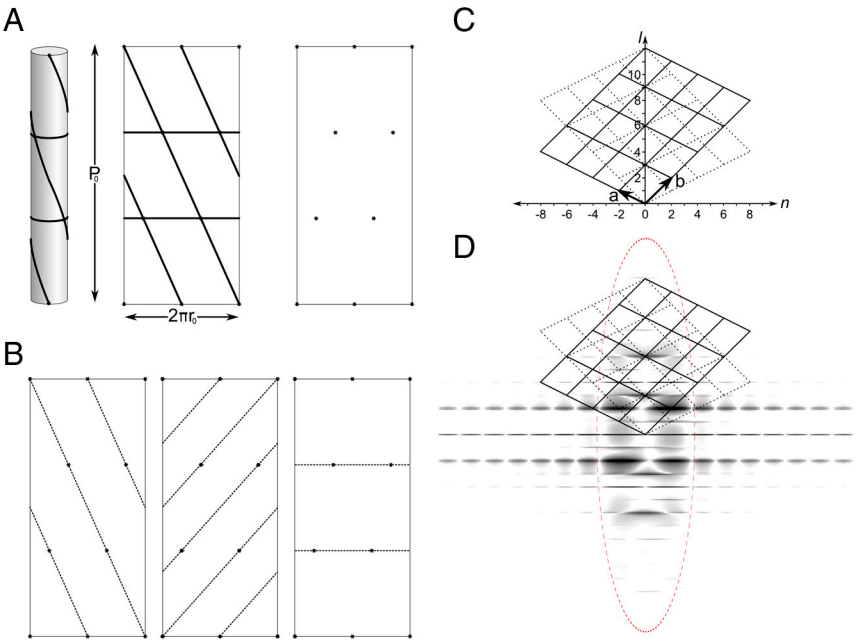

Fig. S6. Indexing and helical reconstruction. (*A*) Helical lattice generation of the SAF-coiled coils. The coiled coil is shown as a cylinder, of radius r_0, with the α-helices coiling up with pitch P_0. Lateral density planes are shown spaced 41.8 Å apart. "Unwrapping" the cylinder allows the helical net to become visible. (*B*) The first and second layer lines (*l*) both describe two-start helices, whereas the third layer line is a zero-order Bessel function. (*C*) Presents *n*, *l* plot describing the Bessel orders present. Arrows "a" and "b" describe the basic lattice vectors, and solid and dashed lines represent the near- and far-side lattices, respectively. (*D*) Lattice overlaid on the Fourier transform of 2dx-processed image. The Fourier transform has been scaled by 25% in the horizontal direction, so the red ellipse traces out 8 Å.

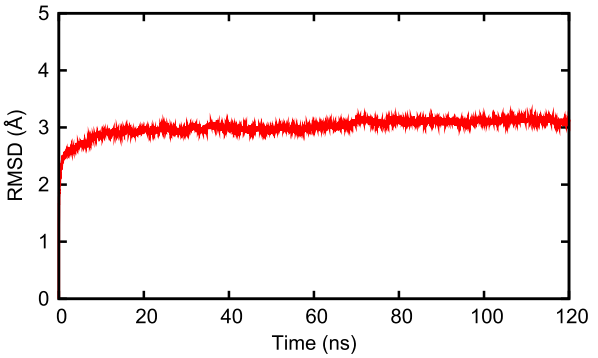

Fig. S7. Rmsd of all backbone and side-chain atoms with respect to the initial energy-minimized model. The graph indicates that the simulation is essentially equilibrated after 20 ns, and the size of the fluctuations is consistent with thermal motions rather than any major conformational change.

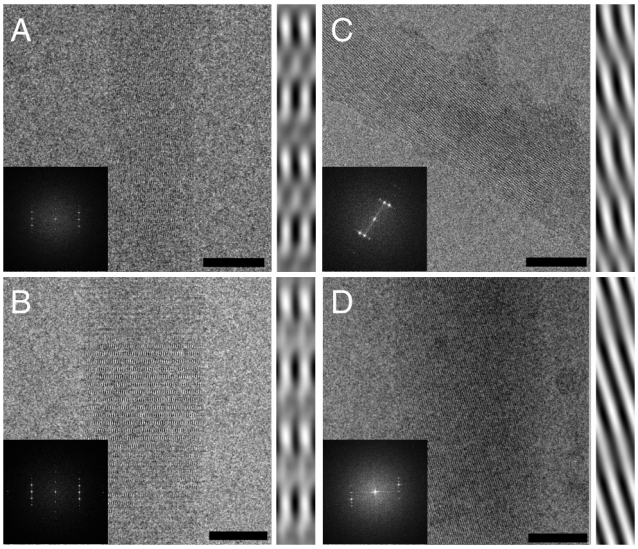

Fig. S8. Fibers processed using 2dx. (*A* and *B*) Fibers with clear lateral and longitudinal striations. (*A* and *B, Insets*) The computed Fourier transform: The first equatorial reflection is at 18 $Å^{-1}$. Processed 2 by 2 unit cells are shown to the right of each image. (*C* and *D*) Fibers with slanted striations, which match model data when the SAF is tilted out of the imaging plane (Fig. 5*C*). All scale bars, 50 nm.

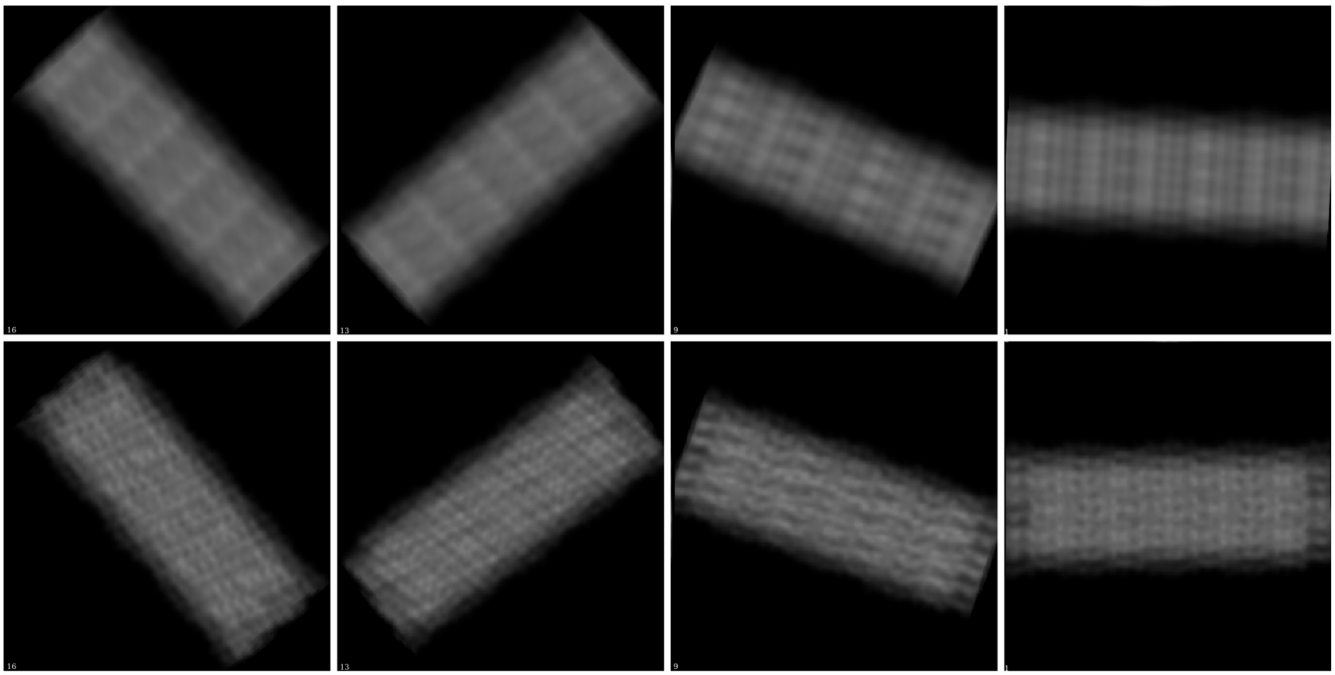

Fig. S9. Lateral striations are visible in a parallel array of coiled coils but not in an antiparallel array. (*Top*) Projections of a model of a parallel array of coiled coils. (*Bottom*) Corresponding projections of an antiparallel array.

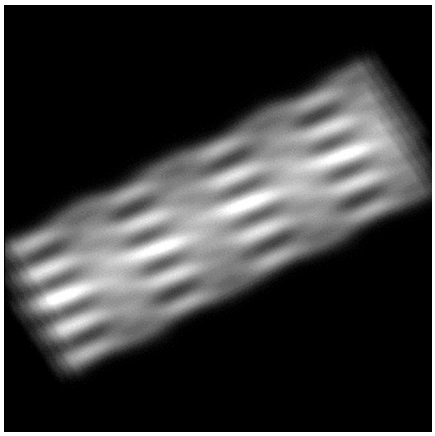

Movie S1. Animation of the SAF model used to simulate projection images. Animated GIF showing projections, separated by 5°, of the all-atom model. The movie shows how the various striations appear at specific rotation and tilt angles.

Movie S1 (GIF)

Table S1. Lattice plane spacing (various lattice planes become visible as a hexagonally packed array is viewed from specific angles)

Plane		Spacing (Å)	Observed?
Unit cell	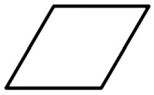	20.8	-
[100]		18	Yes
[110]	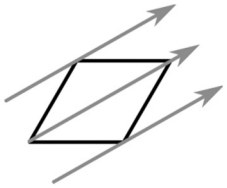	10.4	Yes
[200]	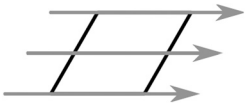	9	Yes
[210]	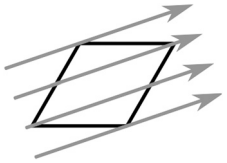	6.8	No
[300]	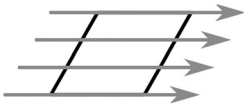	6	Yes

Table S2. SAF peptide sequences and registers

Peptide	Sequence				
Heptad repeat	*g*	*abcdefg*	*abcdefg*	*abcdefg*	*abcdef*
SAF-p1	K	IAALKQK	IASLKQE	IDALEYE	NDALEQ
SAF-p2a	K	IRRLKQK	NARLKQE	IAALEYE	IAALEQ
SAF-p1-I	K	IAALKQK	IASLKQE	IDALEφE	NDALEQ
Blunt-p1-I	E	IDALEφE	NDALEQK	IAALKQK	IASLKQ

The φ in SAF-p1-I represents the *p*-iodo-phenylalanine residue.

Table S3. X-ray diffraction data collection, phasing, and refinement statistics (SAD) for 3RA3

	3RA3
Data collection	
Space group	P 3_2
Cell dimensions	
a, b, c (Å)	45.1, 45.1, 67.6
α, β, γ (°)	90.0, 90.0, 120.0
Resolution (Å)	25.0–2.30 (2.38–2.30)*
R_{merge}	0.102 (0.606)
$I/\sigma I$	21.0 (2.0)
Completeness (%)	99.8 (98.8)
Redundancy	8.2 (5.0)
Refinement	
Resolution (Å)	22.54–2.31
No. reflections #	6767
R_{work}/R_{free}	0.198/0.247
No. atoms	
Protein	857
Waters Ligand/ion	286/1
B-factors	
Protein (main chain/side chains)	47.6/56.5
Waters Ligand/ion	52.782.0/67.7
Rmsd	
Bond lengths (Å)	0.007
Bond angles (°)	0.852

*Highest-resolution shell is shown in parentheses.

Table S4. Layer line Bessel orders

Layer line	Bessel order
1	−2
2	2
3	0
4	−2
5	2
6	0
7	−2
8	2
9	0
10	−2
12	0

Note: The first layer line at 125.4 Å has $n = -2$, describing a left-handed helix.